Int. J. Electrochem. Sci., 15 **(2020)** 6290 – 6301, doi: 10.20964/2020.07.45

International Journal of
ELECTROCHEMICAL
SCIENCE
www.electrochemsci.org

Preparation and Electrochemical Properties of bowl-shaped carbon/molybdenum disulfide composite as cathode material for Lithium Ion Batteries

Zhengping Zhao[1,2], Sitao Shen[2], Yuting Li[2], Qiaodian Chen[1], Xuan Yu[1], Mingqiang Zhong[2] and Xiufang Chen[3,]*

[1] Zhijiang College, Zhejiang University of Technology, Hangzhou, 310014, China
[2] College of Materials Science and Engineering, Zhejiang University of Technology, Hangzhou 310014, China
[3] College of Materials Science and Engineering, Zhejiang University of Science and Technology, Hangzhou 310018, China
[*]E-mail: chenxf@zstu.edu.cn

Received: 4 March 2020 / *Accepted:* 20 April 2020 / *Published:* 10 June 2020

The bowl-shaped polyphosphonitrile nanomaterial was synthesized through a precipitation process, and the surface of the bowl-shaped polyphosphonitrile carbon was loaded with molybdenum disulfide by hydrothermal method. The bowl-shaped carbon@MoS_2 as cathode material for lithium ion batteries is prepared. The specific capacity, cycle stability and discharge performance of lithium ion battery were tested. The results showed that the bowl-shaped carbon@MoS_2 composite had higher specific capacity and better cyclic stability in the charge-discharge test, showing excellent electrochemical performance.

Keywords: Bowl-shaped carbon, Molybdenum disulfide, Cathode materials, Electrochemical properties

1. INTRODUCTION

Energy crisis and environmental pollution have become two important factors hindering the healthy development of today's society. Energy is mainly provided by coal, oil, natural gas and other non-renewable resources. The proven reserves of these resources are limited to a few decades of use. For the huge population base, China has become even more scarce in terms of resources, ranking at the bottom of the world in terms of percapita resources [1-3]. In some cases, it is even less than one fifth of the world's average level. In addition, the combustion and utilization of coal, oil, natural gas and other non-renewable resources will inevitably produce a large number of harmful substances such as SO_2, CO_2, nitrogen oxides and other small particles, which will pollute the atmosphere, generate acid rain, haze and other bad weather, and cause serious pollution to the environment [4-6]. As a pollution-free

energy with a wide range of sources, electric energy has a great application prospect in the new century. However, the storage of electric energy greatly limits the application of electric energy, such as the promotion of electric cars. Electrochemical cell technology is of great interest to researchers in the search for clean, sustainable sources of energy with little or no pollution. Lithium ion batteries with high energy density, long cycle life, no memory effect, large current discharge and high discharge voltage have become the focus of research in various countries and certain research results have been achieved [7-9].

As an important factor restricting the development and performance improvement of lithium ion batteries, cathode materials have been paid more attention. So far, the commonly used cathode materials for lithium ion batteries can be divided into the following kinds: carbon materials, silicon-based materials, tin-based materials, germany-based materials, transition metal oxide materials and transition metal sulfide materials [10-12].

At present, most of the lithium ion batteries in the market use carbon materials such as graphite and metal oxide as the cathode materials of the batteries. Graphite has excellent cycling stability, and the lithium ion batteries formed by it also have high specific capacity and specific power, but their disadvantages are also obvious [13-16]. First of all, the capacity limit of the battery is not ideal enough, and the capacity limit cannot meet the requirements of high specific capacity or be applied to devices that need to work for a long time. Secondly, the deposition potential of lithium metal is close to the embedded lithium potential of lithium ion battery, and lithium metal is likely to produce dendrites on the surface of electrode material, which will precipitate out, causing a short circuit inside the battery and causing potential safety hazards. Third, due to the limitation of graphite or metal oxide performance, the battery with this negative material has poor response to the rapid charging and discharging process. It is difficult to realize the fast charging and high-rate discharge. At present, the performance of lithium ion batteries is far from meeting the requirements of electric vehicles for large capacity and high power batteries. Electrode material is one of the key and core technologies of lithium ion battery technology and an effective means to improve the performance of lithium ion battery. The advantages and disadvantages of electrode materials will directly affect the specific power, specific capacity, cycle times and other electrochemical properties of lithium ion batteries [17-19]. Therefore, the research and development of high performance lithium ion battery electrode materials has become a primary task.

In this paper, a bowl-shaped carbon composite with MoS_2 as cathode material for lithium ion batteries is studied. The bowl-shaped polyphosphonitrile nanomaterial was synthesized through a precipitation process, and the surface of the bowl-shaped polyphosphonitrile was loaded with molybdenum disulfide by hydrothermal method. The specific capacity, cycle stability and discharge performance of lithium ion battery were tested.

2. EXPERIMENTAL SECTION

2.1 Synthesis of cup-shaped polyphosphonitrile nanomaterials (CSPs)

Hexachlorocyclotriphosphazene (0.413 g) and anhydrous phloroglucinol (0.378 g) were weighed and dissolved in 500 ml acetonitrile. Ultrasonic dispersion was conducted for 30 min, and the ultrasonic

power was 450 W. Added 30 ml triethylamine and continue ultrasonic for 150 min. The ultrasonic power is 200 W to get white cloudy liquid. The resulting cloudy liquid was centrifuged and dried to produce a white globular polyphosphonitrile. Grind to powder and set aside. The synthesized globular polyphosphonitrile 0.3 g was weighed, added to 500 ml acetone and ultrasonic 120 min to obtain the cloudy liquid. The cloudy liquid was centrifugally dried and a light yellow bowl-shaped polyphosphonitrile was obtained. Grind to powder and set aside.

2.2 Synthesis of bowl-shaped carbon/molybdenum disulfide composites

0.1 g bowl-shaped polyphosphonitrile, 0.479 g thiourea, 0.3228 g sodium molybdic dihydrate and 57 ml isopropanol were weighed in the reactor, stirred evenly and dispersed by ultrasound for 30 min to obtain a white cloudy liquid. The white cloudy liquid was put into an oven at 180 ºC for reaction for 8 hours and then cooled down naturally. The resulting product was centrifugally dried, that is, the bowl-shaped polyphosphonitrile/molybdenum disulfide composite material. Grind to powder and set aside. The bowl-shaped polyphosphonitrile/molybdenum disulfide composite material was poured into the porcelain boat and put into the tube furnace. Nitrogen was added for 30 minutes and the air was expelled. Then the tube furnace was heated to 900 ℃ under the protection of nitrogen.

2.3 The mainly characterization and testing

FT-IR spectra of all samples were recorded using polymer granule on a Perkin-Elmer Wellesley MA spectrophotometer. Thermogravimetric analysis (TGA) was performed on a TGA 7 instrument (PerkinElmer) thermal analysis system. Sample weight taken was 2-4 mg. All the experiment data were taken as an average of at least five measurements. The microstructures were observed on a Scanning Electron Microscope (Hitachi S4000, Japanese) and a Transmission Electron Microscope (JEM-100CX II, Japanese). Raman spectroscopy is a method for qualitative analysis of molecular structure. The chemical structures were observed on a Lab RAM HR UV800 laser Raman spectrometer (JOBIN YVON, France). The excitation light source is 632.81 nm and the scanning range is 200~4000. The XPS (KRATOS AXIS Ultra DLD, Shimazu KRATOS) was used. The light source was AI-KaX rays and the vacuum degree was $3*10^{-7}$ Pa. Nitrogen adsorption test (BET) was using the automatic physical adsorption instrument (ASAP2020, mack instruments). X-ray diffractometer (X'pert PRO, PANalytical) was used. The test parameters of the instrument are as follows: 36 kV, 30 mA and Cu radiation.

The constant charge-discharge performance was tested after the sample electrode material was assembled into CR 2025 button battery. The electrochemical performances such as power density, energy density and specific capacitance can be obtained by processing and analyzing the results of constant current charge-discharge test [20]. The calculation formula of specific capacitance is:

$$Cs = I\Delta t/m\Delta V \quad (1\text{-}1)$$

Where I(A) is the charge-discharge current. Δt for discharge time. m is the mass of the active substance in the electrode material. ΔV is the discharge voltage range.

The cyclic voltammetry is to discuss the reaction of capacitor electrode after applying triangular

waveform potential. The applied control signal is potential, and the measured corresponding signal is current. It is mainly to study the change rules of I-t and I-U. The relation curve of U-I can be obtained by observing the T-t graph [21].

3. RESULTS AND DISCUSSION

Figure 1 is the microtopography of spherical polyphosphonitrile at different multiples. As can be seen from the figure, polyphosphonitrile microspheres with a diameter of 500 nm and a relatively uniform size can be prepared under ultrasonic conditions from hexachlorocyclotriphosphazene and phloroglucinol as raw materials and triethylamine as acid binding agent.

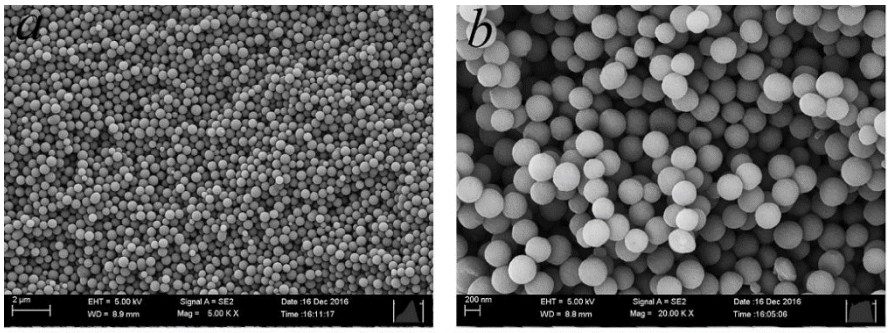

Figure 1. The microtopography of polyphosphonitrile microspheres

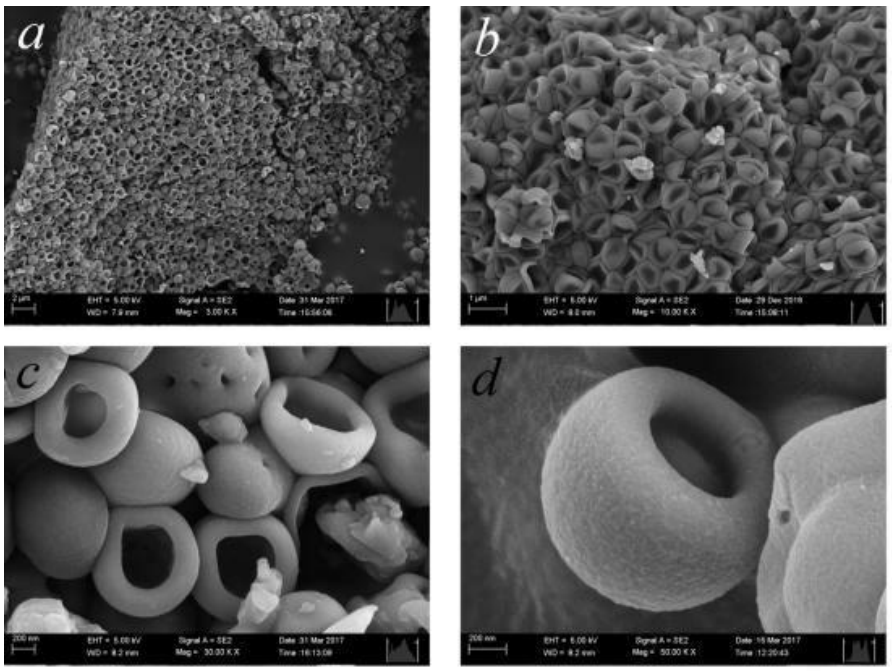

Figure 2. The microtopography of bowl-shaped polyphosphonitrile

Figure 2 is microtopography of cup-shaped polyphosphonitrile corroded with acetone. It can be seen from the figure that the spherical polyphosphonitrile etched into a bowl under the action of acetone. Compared with spherical polyphosphonitrile, bowl-shaped polyphosphonitrile has a larger specific surface area. After surface loading of molybdenum disulfide, the specific surface area is larger than that of spherical polyphosphonitrile/MoS_2 composites, which can be expected to have better electrochemical properties.

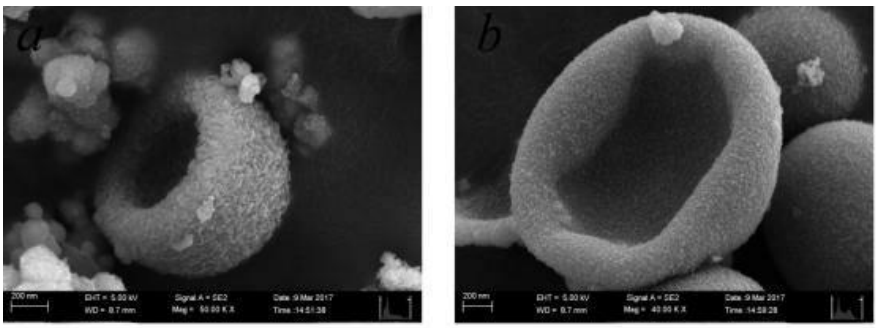

Figure 3. The microtopography of of bowl-shaped polyphosphonitrile@MoS_2

Figure 3 is the microtopography of bowl-shaped carbon material/MoS_2 composite material formed after sintering at high temperature. It can be seen that lamellar molybdenum disulfide grows on the surface of bowl-shaped carbon material [22]. However, there are still a small amount of molybdenum disulfide aggregates to form particles.

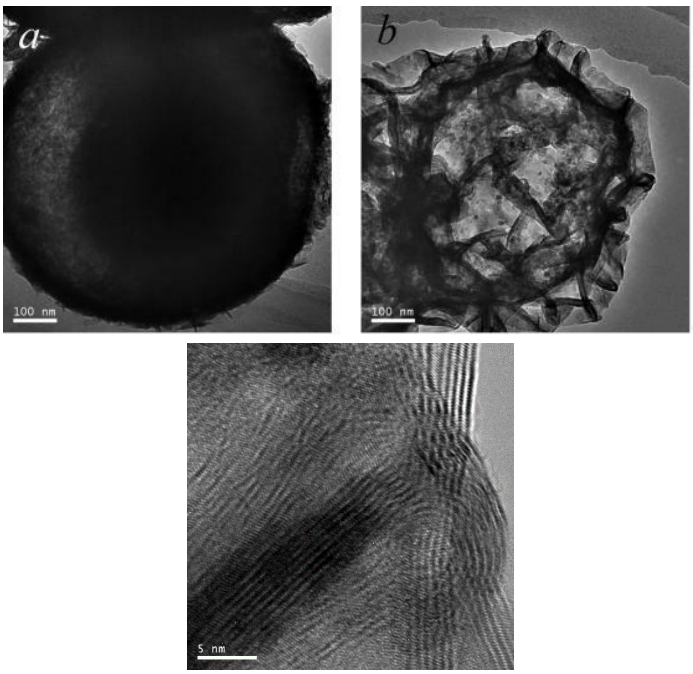

Figure 4. The microtopography of bowl-shaped carbon/MoS_2 composite

Figure 4 shows the transmission electron microscopy of bowl-shaped carbon/molybdenum disulfide composites. As can be seen from the figure, the color of the middle and edge areas is slightly darker, while the color of other areas is slightly brighter. After carbonization, the composite material presents a bowl-like structure unchanged. The composite material has roughly interlaced carbon chains inside that act as the backbone for the entire bowl-shaped composite [23]. Flake molybdenum disulfide grows on the surface of composite material, and the boundary between molybdenum disulfide and carbon material is obvious. A thin layer of molybdenum disulfide grew on the surface of the carbon bowl. The lamellar molybdenum disulfide grows outward with a length of about 70 nm, lamellar spacing of about 100 nm, and lattice spacing of molybdenum disulfide of 0.62 nm.

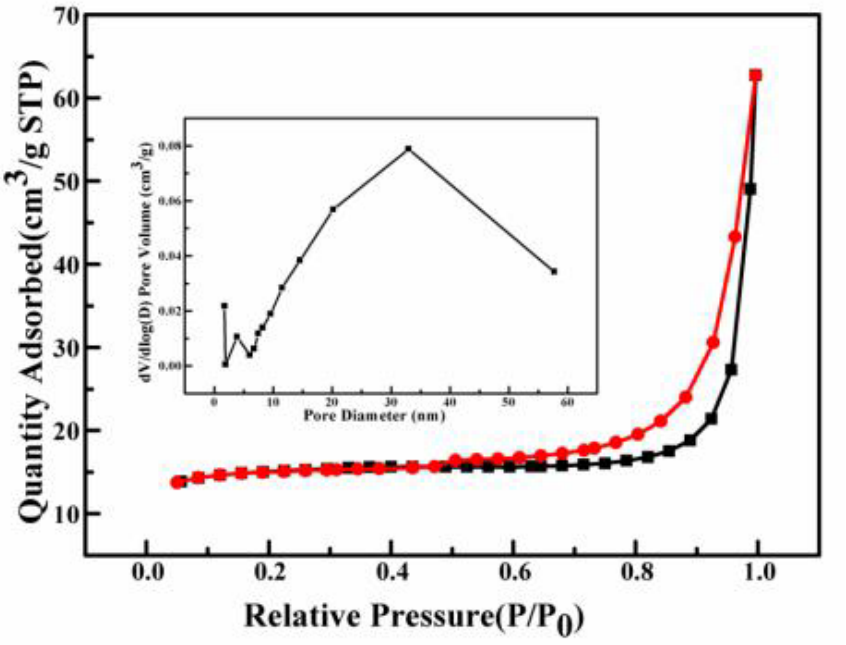

Figure 5. Nitrogen sorption-desorption curve and pore size distribution of bowl-shaped carbon/MoS_2 composite

Table 1. The specific surface area, pore volume and pore diameter of the cathode materials

CODE	BET (m^2/g)	pore volume (cm^3/g)	BJH adsorption average aperture (nm)	BJH desorption average aperture (nm)
MoS_2 [24]	5.93	0.003	349.9	185.5
Spherical carbon [25]	4.44	0.002	342.1	167.1
Spherical carbon/MoS_2 [26]	33.52	0.013	222.5	198.2
Bowl-shaped carbon/MoS_2	46.64	0.019	242.3	209.0

Figure 5 shows the nitrogen sorption-desorption curves and pore size distribution of the sample.

The figure shows that the sample of nitrogen adsorption curves are IV shaped. Under the strong low pressure, the curve is gentle and the rise is not obvious. As the pressure increases, the curve goes up faster, suddenly steepens, and then explosively. It is indicates that a large number of microporous structures in the sample. The high-pressure growth of nitrogen absorption and desorption curve is due to the mesoporous effect of nitrogen in the micropores of the sample, which causes a large amount of nitrogen to accumulate in the nanoscale pores of the sample and resulting in the extreme rise of the curve. It can be seen from the pore size distribution that the pore size of the sample is nanometer. Table 1 shows the specific surface area, pore volume and pore diameter of the sample. As can be seen from the table, the specific surface area of bowl-shaped carbon composite molybdenum disulfide is much higher than that of pure molybdenum disulfide, and the pore diameter is nanometer [27]. The bowl-shaped carbon/molybdenum disulfide composite has a large specific surface area and can exhibit better electrochemical properties.

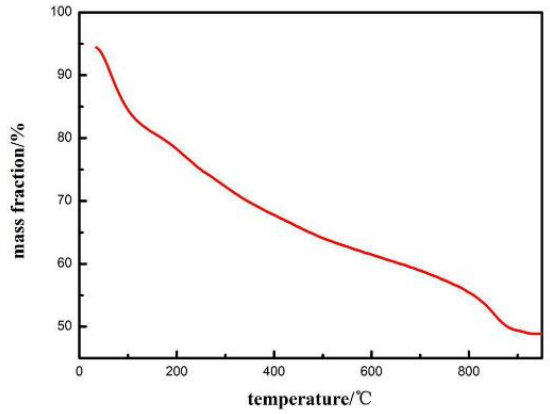

Figure 6. TGA curves of bowl-shaped polyphosphonitrile/MoS_2 composites

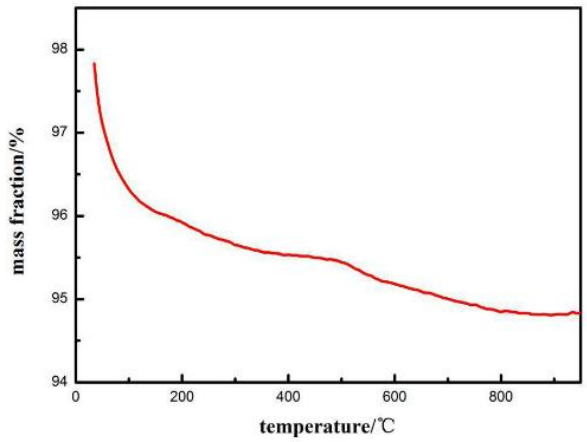

Figure 7. TGA curves of bowl-shaped carbon/MoS_2 composites

Figure 6 shows the thermogravimetric analysis of bowl-shaped polyphosphonitrile/MoS_2

composites. As can be seen from the figure, the bowl-shaped polyphosphonitrile/MoS_2 composite began to decompose at 100 ºC and finished at 900 ºC, with mass loss of about 60%-70%. Figure 7 shows the thermogravimetric analysis curve of the bowl-shaped carbon material/molybdenum disulfide composite material after high temperature sintering at 900 ºC. It can be seen from the figure that there is basically no mass loss in the heating process of the composite material after high temperature treatment, indicating that the treatment temperature of 900 ºC is reasonable and the target bowl-shaped carbon material/MoS_2 composite material can be obtained.

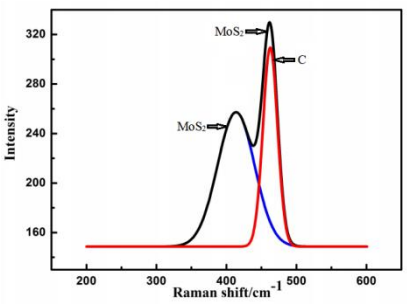

Figure 8. Raman spectra of bowl-shaped carbon/MoS_2 composites

Figure 8 shows the Raman spectra of bowl-shaped carbon/MoS_2 composites. There are five vibration modes of MoS_2, but only two vibration modes, namely E^1_{2g} and A_{1g}, remain due to the restriction and selection rules of Rayleigh scattering radiation and the effect of Raman properties [28]. As can be seen from the figure, A_{1g} is an out-of-plane vibration and E^1_{2g} is an in-plane vibration. The spectral peak position of molybdenum disulfide in Raman spectrogram is closely related to the number of layers and the aggregation of MoS_2. As the number of MoS_2 layers increases, the van der Waals force between layers decreases, and the vibration mode E^1_{2g} red shifts, while A_{1g} red shifts. The E^1_{2g} peak of monolayer MoS_2 is around 385 cm^{-1}, while the A1g peak is around 403. As can be seen from the figure, the first two peaks are the peaks of MoS_2. The two peaks are located at 410 cm^{-1} and 460 cm^{-1}, respectively, so the MoS_2 in the sample is confirmed to be in a multi-layered form. C

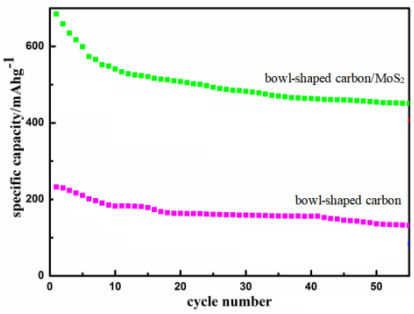

Figure 9. The cycle times and discharge specific capacity of the cathode materials

Figure 9 shows the curve of the cycle times and discharge specific capacity of the sample. Because the sample is pure carbon material, the specific capacity is low, only 100-200 $mAH \cdot g^{-1}$. Compared with pure carbon materials, the specific capacity of composite carbon materials after MoS_2 has been significantly improved. The specific capacity of bowl-shaped carbon material MoS_2 composite has reached 500 $mAH \cdot g^{-1}$, and the cycling stability is relatively good [29]. The comparsion of bowl-shaped carbon/MoS_2 composites and other anode materials were added in table 2.

Table 2. The specific capacity comparison of several common cathode materials

Cathode materials	Capacity ($mAh \cdot g^{-1}$, 50 cycles)	Retention rate (%, 50 cycles)
Petroleum carbon [6]	264	77.0
MoS_2@carbon [8]	387	78.2
Si@carbon [12]	1213	68.3
This work	496	81.1

As can be seen from table 2, traditional petroleum carbon anode materials have a lower specific capacity and the corresponding 50 cycle retention rate is also low. It is also verified that only the embedding and stripping of lithium ions exist in the charging and discharging process of petroleum carbon anode materials. The specific capacity of the battery is also proportional to the graphitization degree of the carbon material. The higher the graphitization degree, the higher the specific capacity. However, its maximum specific capacity is 372 $mAh \cdot g^{-1}$, which is much lower than the application of transition metal or metal oxide as anode material [6]. MoS_2 has the highest specific capacity, which is 865 $mAh \cdot g^{-1}$ after 50 charge and discharge cycles, but has the defect of large expansion coefficient [14]. However, in the charging and discharging process of metallic MoS_2, the embedding and ejection of lithium ions tend to lead to metal embrittlement, resulting in a significant reduction in specific capacity. Silicon and its composite carbon materials have high specific capacity, but their embrittlement cracking is serious and the specific capacity retention rate is low. Compared with molybdenum disulfide, both they each has advantages and disadvantages. There are many negative electrode materials that cannot be listed one by one. However, polyphosphonitrile carbon has a broad application prospect in the field of new energy batteries due to its strong molecular design and excellent electrochemical properties.

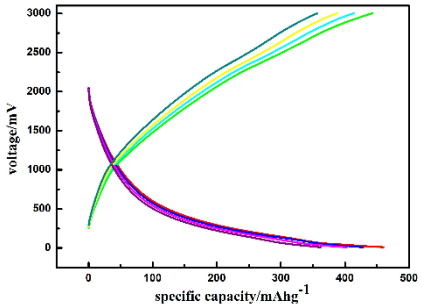

Figure 10. The capacitive voltage curve of bowl-shaped carbon cathode materials

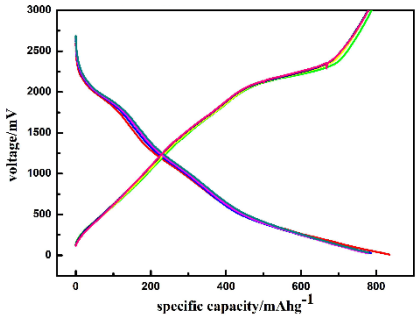

Figure 11. The capacitive voltage curve of bowl-shaped carbon/MoS_2 cathode materials

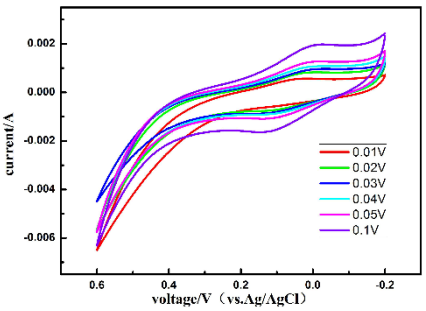

Figure 12. The capacitance-voltage curve of bowl-shaped carbon cathode materials

Figure 12 shows the capacitance-voltage curve of the sample. As can be seen from the figure, the bowl-shaped carbon material/MoS_2 has a higher specific capacity. During the charging process, there is a platform at the voltage of 2100 mV where lithium ions are embedded into the cathode material. During the discharge process, there are two platforms at the voltage of 2000 mV and 1100 mV, which are platforms for lithium ions to escape from the cathode material [30].

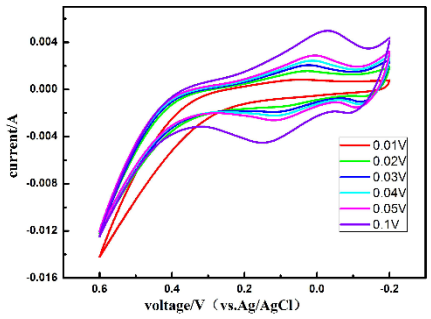

Figure 13. The capacitance-voltage curve of bowl-shaped carbon/MoS_2 cathode materials

Figure 13 shows the cyclic voltammetry curve of the samples. Each sample is the cyclic voltammetry curve measured at the scanning rates of 0.01 V/S, 0.02 V/S, 0.03 V/S, 0.04 V/S, 0.05 V/S and 0.1 V/S. The bowl-shaped carbon/MoS_2 composite material contains the highest power and the best electrical performance. In addition, the higher the scan rate, the less power it contains. From the cyclic voltammetry curve of the molybdenum disulfide loaded samples, it can be seen that the curve has obvious fluctuation, which indicates that the redox reaction occurred during the cycle.

4. CONCLUSIONS

Polyphosphonitrile obtained from hexachlorocyclotriphosphazene and anhydrous phloroglucinol was used as carbon source. It was confirmed that the surface supported sheet MoS_2 bowl-shaped carbon material was prepared successfully and that the MoS_2 coated on the bowl-shaped carbon material was indeed lamellar. Through the charge-discharge performance test and cyclic voltammetry test, it can be obtained that the bowl-shaped carbon material/MoS_2 composite material has better electrochemical performance.

ACKNOWLEDGEMENTS
We are thankful for Project Supported by Zhejiang Provincial Natural Science Foundation of China (Grant No. LY18E030009) and the National Natural Science Foundation of China (No. 21504079) for the support to this research.

References

1. C. Wellum, *Enterp. Sco.* 21 (2020) 2.
2. K. Andriosopoulos, E. Galariotis and S. Spyrou, *Energ. Econ.,* 66 (2017) 217.
3. E. Kolasi, *Mon. Rev.*, 71 (2019) 31.
4. F. EI Ouardighi, K. Kogan, G.Gnecco and M. Sanguineti, *An. Oper. Res.*, 287 (2020) 653.
5. G. Manjula and M. Seenuvasan, *J. Environ. Biol.*, 40 (2019) 1.
6. J. M ori, A. Fini, M. Galimberti, M. Ginepro, G. Burchi, D. Massa and F. Ferrini. *Sci. Total Environ.*, 643 (2018) 725.
7. C.W. Lee, H.S. Kim and S.I. Moon, *Mater. Sci. Eng. B*, 123 (2005) 234.

8. P. Peng, Y. Sun and F. Jiang, *Heat Mass Transfer*, 50 (2014) 1405.
9. Z.P. Zhao, J.J. Hu, Z.P. Zhou and M.Q. Zhong, *Optoelectron. Adv. Mat.*, 10 (2016) 117.
10. F. Nobili, F. Croce and R. Tossici, *J. Power Sources*, 197 (2012) 276.
11. P. Ghosh, S. Mahanty and R.N. Basu, *Electrochim. Acta*, 54 (2009) 1654.
12. G.L. Zeng, W. Zhou, J.L. Zheng, Z.H. Fan and H. Chen. *J. Nanosci. Nanotechno.*, 20 (2020) 4899.
13. M.M. Radhi, W.T. Tan, M.Z. Rahman and A.B. Kassim, *Int. J. Electrochem. Sci.*, 5 (2010) 254.
14. Z.P. Zhao, S.T. Shen, M.Q. Zhong and X.F. Chen, *Int. J. Electrochem. Sci.*, 15 (2020) 3846.
15. B.F. Ji, W.J. Yao, Y.P. Zheng, P. Kidkhunthod, X.L. Zhou, S. Tunmee, S. Sattayaporn, H.M. Chen, H.Y. He and Y.B. Tang, *Nat. Commun.*, 11 (2020) 1225.
16. H.H. Chung, H.C. Wu and N.L. Wu, *Electrochem. Commun.*,10 (2008) 1823.
17. Y.D. Cho, G.T.K. Fey and H.M. Kao, *J. Solid State Electr.*, 12 (2008) 815.
18. Z.P. Zhao, S.T. Shen, M.Q. Zhong and J.W. Chew, *Int. J. Electrochem. Sci.*, 14 (2019) 10058.
19. T.Takamura, S. Ohara M. Uehara, J.Suzuki and K. Sekine, *J. Power Sources*, 129 (2004) 96.
20. Y. G. Li, B. Tan and Y. Y. Wu, *Nano Lett.,* 8 (2008) 265.
21. B.Wang, X. L. Wu, C. Y. Shu, Y. G . Guo and C . R.Wang, *J. Mater. Chem.,* 20 (2010) 10661.
22. H.L.Wang, L.F. Cui, Y.A. Yang, H.S. Casalongue, J.T. Robinson, Y.Y. Liang, Y. Cui and H.J. Dai, *J. Am. Chem. Soc.,* 132 (2010) 13978.
23. Z.P. Zhao, S.T. Shen, M.Q. Zhong and J.W. Chew, *Int. J. Electrochem. Sci.*, 15 (2020) 2739.
24. Z.S. Wu, W.C. Ren, D.W. Wang, F. Li, B.L. Liu and H.M. Cheng, *ACS Nano*, 4 (2010) 5835.
25. J. Yao, X.P. Shen, B. Wang, H.K. Liu and G.X. Wang, *Electrochem. Commun.,* 11 (2009) 1849.
26. J.K. Lee, K.B. Smith, C.M. Hayner and H.H. Kung, *Chem.Commun.*, 46 (2010) 2025.
27. K. Chang and W.X. Chen. *J. Mater. Chem.,* 21 (2011) 17175.
28. K.F. Mak, C. Lee and J. Hone, *Phys. Rev. Lett.,* 105 (2010) 136805.
29. H. Liu, M. Si and S. Najmaei, *Nano lett.*, 13(2013) 2640.
30. K. Chang and W.X. Chen, *J. Mater. Chem.*, 21 (2011) 17175.